



This is a repository copy of *Influence of testing temperature on the mechanical performance of brazed conventionally and additively manufactured 316L stainless steel joints*.

White Rose Research Online URL for this paper:

<https://eprints.whiterose.ac.uk/227328/>

Version: Published Version

---

**Article:**

Livera, F., Charvet, R., Hind, N. et al. (5 more authors) (2025) Influence of testing temperature on the mechanical performance of brazed conventionally and additively manufactured 316L stainless steel joints. *Advanced Engineering Materials*. 2500323. ISSN 1438-1656

<https://doi.org/10.1002/adem.202500323>

---

**Reuse**

This article is distributed under the terms of the Creative Commons Attribution (CC BY) licence. This licence allows you to distribute, remix, tweak, and build upon the work, even commercially, as long as you credit the authors for the original work. More information and the full terms of the licence here:

<https://creativecommons.org/licenses/>

**Takedown**

If you consider content in White Rose Research Online to be in breach of UK law, please notify us by emailing [eprints@whiterose.ac.uk](mailto:eprints@whiterose.ac.uk) including the URL of the record and the reason for the withdrawal request.



[eprints@whiterose.ac.uk](mailto:eprints@whiterose.ac.uk)  
<https://eprints.whiterose.ac.uk/>

# Influence of Testing Temperature on the Mechanical Performance of Brazed Conventionally and Additively Manufactured 316L Stainless Steel Joints

Frances Livera, Raphaël Charvet, Neil Hind, Sophie Barwick, Dennis Premoli, Iain Todd, Andreas Mortensen, and Russell Goodall\*

In this work, brazed joints between samples of 316L stainless steel (316LSS) are formed using the Ag155 brazing filler metal. As an additional aspect of the investigation, the joints combine stainless steel formed by conventional processing and by additive manufacture (AM). These samples are then tested to determine their shear response with temperature, employing a bespoke test design comprising a set of three cylindrical samples held together with two brazed joints. Multiple samples are tested at 20 and 500 °C and single samples at intermediate temperatures. A shear strength above 200 MPa is retained up until 200 °C, and, despite significant differences in steel microstructure, the conventional or AM processing of the 316LSS does not affect joint failure. At higher temperatures, there is a progressive decrease in both the failure strength and the ductility of the joint. The reasons for the behavior are traced to changes, potentially associated with a transformed layer in the steel near to the joint, in the operating failure mechanism as determined by observations of the failure surfaces of the joints. These results highlight the importance of systematic investigations of the strength of brazed joints with temperature and correlation of these to the joint microstructure.

of different size, without part distortion or significant change in microstructure. Thus, brazing has been employed in a varied set of applications, including the joining of advanced materials subject to elevated operating temperatures.

The performance of these joints under non-ambient conditions is important and often nontrivial. It is known that the formation (and subsequent elevated temperature behavior) of brazed joints involves a number of steps and different interactions, which depend on the materials being joined, on the alloy that is melted between them (the filler metal) to form the joint, and of course on the temperature. These processes are discussed in detail in Ref. [1]. In some cases, interdiffusion produces the joint, while in others (especially, but not always, in joints involving a ceramic material), it is the formation of an interfacial reaction layer that ensures sufficiently

## 1. Introduction

The versatility of brazing as a joining method provides unique capabilities unmatched by other bonding techniques. It can, for example, provide metallic joints, which are electrically and thermally conductive, relatively strong, and resistant to different environments and elevated temperatures, between components

intimate and strong bonding across the joint. Such layers can have a critical effect on the quality of the joints, also in metallic systems; Ref. [2] gives an example. Other phenomena, not critical for joint formation but producing effects which can impact joint performance, can also occur during brazing. For example, in the brazing of 304 stainless steel with Cu-based filler metals, a degree of dissolution of the steel occurs. This results in the precipitation of fine Fe inclusions in the filler metal, which often display complex dendritic morphologies.<sup>[3,4]</sup>

While there is some understanding in the industry of how standard grades of brazing alloys, known as filler metals, behave at elevated temperatures, there are relatively few reports of brazed joint mechanical property assessments other than at room temperature.<sup>[5–8]</sup> In order to provide some understanding of how the properties of a commonly used filler metal change with temperature, a bespoke specimen geometry was used here to conduct a series of tests that measure the impact of increased service temperature on the joint strength. For this work, Ag155 (55Ag21Cu22Zn2Sn) was selected as the filler metal, as this is widely used for joining a diverse range of substrates. It is here used to bond samples of 316L stainless steel (316LSS), another commonly used material. The effect of processing of the stainless steel on the joint strength is furthermore investigated by bonding conventionally manufactured 316LSS to

F. Livera, N. Hind, S. Barwick, D. Premoli, I. Todd, R. Goodall  
School of Chemical, Materials and Biological Engineering  
University of Sheffield  
Mappin St, Sheffield City Centre, Sheffield S1 3JD, UK  
E-mail: r.goodall@sheffield.ac.uk

R. Charvet, A. Mortensen  
Laboratory of Mechanical Metallurgy  
École Polytechnique Fédérale de Lausanne (EPFL)  
Lausanne 1015, Switzerland

 The ORCID identification number(s) for the author(s) of this article can be found under <https://doi.org/10.1002/adem.202500323>.

© 2025 The Author(s). Advanced Engineering Materials published by Wiley-VCH GmbH. This is an open access article under the terms of the Creative Commons Attribution License, which permits use, distribution and reproduction in any medium, provided the original work is properly cited.

DOI: 10.1002/adem.202500323

316LSS made via additive manufacturing (AM), with both samples ground to the same surface finish prior to joining. The use of these different manufacturing processes significantly affects the material microstructure: In AM processing, the rapid solidification rates and high thermal gradient, coupled with the remelting of the underlying layer of previously solidified material, lead generally to directionally grown fine-scale structures, similar to welded microstructures, with epitaxial growth often allowing grain size to exceed the layer thickness; reviews of the subject can be found in Ref. [9,10] In AM 316LSS produced by laser powder bed fusion (LPBF) specifically, the structure is fully austenitic with a hierarchical microstructure spanning five to six orders of magnitude encompassing oxide inclusions, solidification cells, and fusion boundaries, together with high- and low-angle grain boundaries.<sup>[11]</sup> Comprehensive reviews specific to AM-processed steel can be found in Ref. [12,13] The use of AM-processed material has been shown to affect the structure of brazed joints,<sup>[14]</sup> so the investigation of their impact on the brazed joint mechanical behavior was viewed as technologically relevant.

## 2. Experimental Section

The sample design is comprised of a stack of three  $\text{\O} 7.5 \text{ mm} \times 5 \text{ mm}$  316LSS cylinders brazed together with two  $\text{\O} 10 \text{ mm}$ ,  $250 \mu\text{m}$  Ag155 (55Ag21Cu22Zn2Sn) braze alloy disks. The end cylinders in the stack were machined, conventionally processed 316LSS, while the central cylinder was additively manufactured, resulting in a symmetrical joint system (all cylinders were ground to the same surface finish, removing the rough surface that results from the AM process). The machined 316LSS  $\text{\O} 8 \text{ mm}$  rod, which was sectioned into 5 mm long cylinders,

was provided by Goodfellow Cambridge Ltd, UK. The Ag155 filler metal was provided by VBC Group, Loughborough, UK.

The sample and testing rig are shown schematically in **Figure 1**. The present test method offered some advantages over other techniques that were often used for the assessment of the shear strength of brazed joints. Lapped shear samples were often the basis for industry standard tests, but these required relatively large amounts of material, both in terms of the filler needed to create the joint and also in terms of the amount of base material to be joined. These requirements could be problematic during early stages of material development, when the quantities of material accessible might be low. Another test that was used in this situation was the cylinder-on-plate test introduced by Matsu et al.<sup>[15]</sup> While the volume of material required is lower, this sample is asymmetrical and does not generate pure shear at the interface. The design used here offers some advantages over these methods; however, it is not perfect either, given the presence of edge effects,<sup>[16]</sup> which are neglected here. Also, there are aspects that need care in experimentation; for example, it is important that in brazing, the cylinders be kept parallel and well aligned unless final machining of the cylinder shown in Figure 1 is to be conducted after joining.

### 2.1. AM of 316LSS Cylinder

AM cylinders of  $\text{\O} 8 \text{ mm} \times 5 \text{ mm}$  were manufactured on an Aconity3D Mini via L-PBF under an argon atmosphere. The samples were built horizontally, such that the footprint on the base-plate was circular. The gas-atomized 316LSS powder feedstock, supplied by Carpenter Additive, had a median size of  $21.4 \mu\text{m}$  ( $D_N 10$  of  $15.2 \mu\text{m}$ ,  $D_N 90$  of  $32.1 \mu\text{m}$ ). During manufacture, the laser was set to a meandering scan strategy at  $150 \text{ W}$  and  $800 \text{ mm s}^{-1}$ , with an initial scan angle of  $22.5^\circ$  and a  $70^\circ$

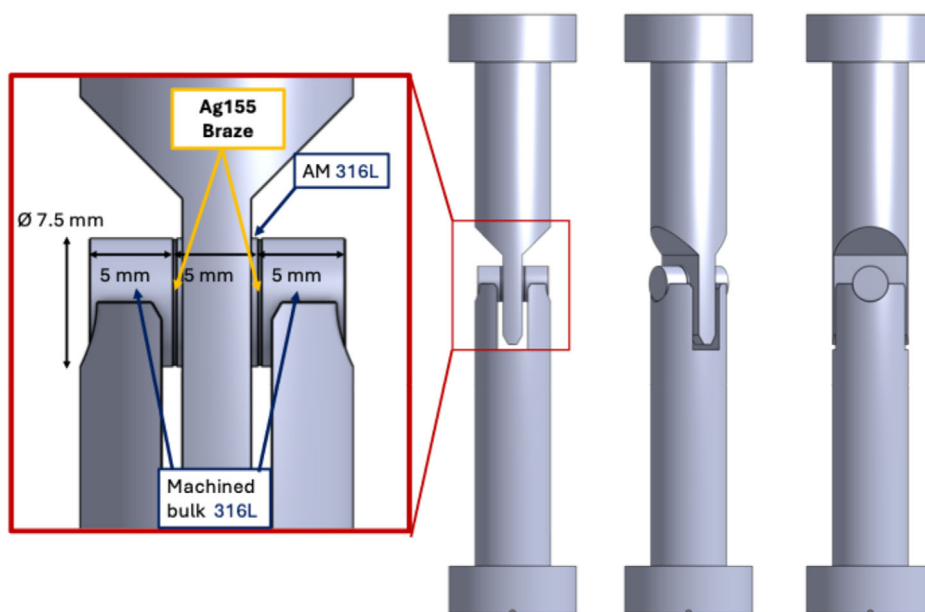


**Figure 1.** A schematic diagram of the configuration of the samples and testing rig. In testing, the edge cylinders are supported in semicylindrical grooves, while another machined shape applies pressure to the central cylinder, setting up shear stress across the joints.

increment. The hatch spacing was 0.080 mm, and the layer thickness was 0.030 mm. The contour laser parameters were 150 W, 1200 mm s<sup>-1</sup>, and an offset of 0.070 mm. The cylinders were removed from the base plate via electron discharge machining and submerged in an isopropanol ultrasonic bath for 15 min to remove excess powder.

## 2.2. Air Furnace Brazing

All of the cylinders were ground with a P1200 grit paper to a standard surface finish ahead of the brazing process, resulting in an average surface finish roughness ( $S_a$ ) of 1.66  $\mu\text{m}$  for the machined cylinders and 1.86  $\mu\text{m}$  for the AM cylinders. Air furnace brazing was completed at 680 °C for 20 min using Ag155 and Tenacity 5 flux (Johnson Matthey, Royston, UK), where the samples were placed directly into the furnace at the brazing temperature. Once air cooled, samples were grit-blasted to remove excess flux and surface oxides and then machined on a lathe to a 7.5 mm diameter to ensure a consistent shape.

## 2.3. Microstructural Characterization

Scanning electron microscopy (SEM) coupled with energy dispersive X-ray spectrometry (EDS) was completed on a FEI Inspect F50, operating at 20 kV and a 10 mm working distance. Samples were ion etched with a Gatan PECS II ahead of electron backscatter diffraction (EBSD) on a JEOL JSM-7900 F with an Oxford Instruments Advanced Symmetry System EBSD detector, operating at 20 kV and a 13 mm working distance. Samples were scanned with a step size of 0.2  $\mu\text{m}$  and a specimen tilt of 70°, and data were obtained using the AZtec HKL software, indexing copper,  $\alpha$ -iron (BCC), and  $\gamma$ -iron (FCC) from the HKL database. Macroscopic fractographs were taken using a Canon 90D DSLR camera and 100 mm F2.8 CA-DREAMER Macro 2X lens.

## 2.4. Mechanical Testing

Room and high-temperature shear testing of the brazed joints was completed on a MFL EZU100 100 kN tensile testing apparatus, with the tensile sample surrounded by a lamp furnace (Research Inc., Model 4068-12-10) at 20, 100, 200, 250, 300, 400, or 500 °C. Two samples were tested at 20 °C, three at 500 °C, and a single sample at each of the intermediate conditions. Heating rates were  $\approx 3\text{ }^\circ\text{C s}^{-1}$ , and the temperature was controlled by a thermocouple placed in contact with the sample. The tests were carried out in air. Figure 1 provides a description of the test and sample configurations. The sample rests along its two outer (machined 316LSS) edge cylinders onto semicircular grooved steel supports. Upon testing, load is applied on the central cylinder via a similar semicircular steel groove, such that pressure is distributed across the entire upper or lower surface of the centre and edge cylinders, respectively. A downward initial load of 0.1 kN was applied to the central cylinder ahead of heating. Once the temperature stabilized at the target temperature  $\pm 5\text{ }^\circ\text{C}$  for 1 min, the sample was incrementally loaded at 0.01 mm s<sup>-1</sup> to failure.

## 3. Results and Discussion

### 3.1. Joint Microstructure

SEM images of the joint cross section in samples that were not loaded are shown in Figure 2. The microstructure of the joint braze alloy region is composed of larger Cu-based regions (medium grey) and a eutectic phase that combines an Ag-based solid solution (light grey) and a Cu-based solid solution, as highlighted by the EDS maps. This is consistent with literature examples of similar Ag–Cu-based brazing systems.<sup>[6,17]</sup> There is little interaction between the 316LSS and Ag155, but a layer of fine grains is present at the interface of the filler metal with both the AM and machined 316LSS that forms during brazing.

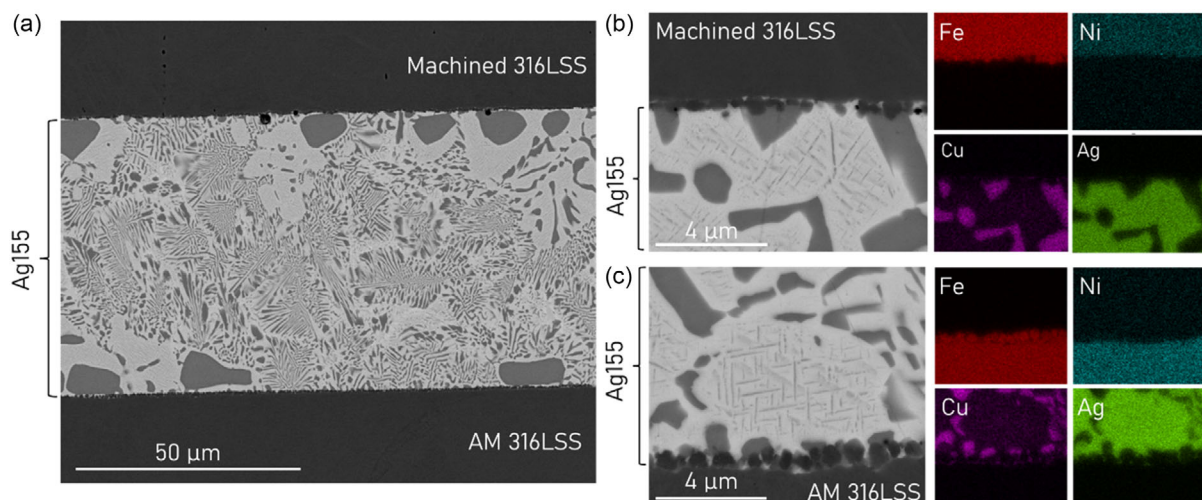


**Figure 2.** a) SEM image of the Ag155 joint cross section (taken from near the middle of the joint depicted in Figure 1, in samples that had not been loaded) with AM 316LSS at the top and machined 316LSS at the bottom, higher magnification SEM images and corresponding EDS maps of Fe, Ni, Cu, and Ag of the interface between Ag155 and b) machined 316LSS and c) AM 316LSS.

EDS maps show that the average composition of the layer (dark grey) does not feature Cu or Ag, but is rich in Fe, so it must be steel-based and originate from the stainless steel. Interestingly, the fine grains are depleted in Ni.

An examination of the interfacial region via EBSD in **Figure 3** reveals that the fine grains are formed of a body-centered cubic (BCC) Fe phase. BCC-Fe is also observed at a small volume fraction in the machined 316LSS, which can indeed contain residual ferrite.<sup>[18]</sup> Usually, 316LSS and the Ag155 filler metal have face-centered cubic (FCC) crystal structures. The difference in the grain structure of the stainless steel with processing route is visible, with the AM material having elongated columnar grains, while grains in the conventionally processed 316LSS are equiaxed and slightly twinned. There is no clear orientation relationship between the BCC-Fe grains and the base material or the filler metal. A similar BCC-Fe interfacial layer has been shown to form during the brazing, using a CuGeNi braze alloy, of austenitic stainless steels by Livera,<sup>[14]</sup> who further also noted a suppression of the BCC-Fe phase formation in AM 316LSS.

In the present case, the formation of the BCC-Fe layer is likely caused by local interdiffusion along the interface during brazing, with Ni diffusing out from the 316LSS into the Ag155 upon contact with the liquid filler metal and Zn moving from the filler into the steel. Such an interaction has been studied by Sage and Fink,<sup>[19]</sup> who showed the effects of liquid Zn spreading on

304SS, which resulted in the formation of a BCC-Fe layer revealed by EBSD analysis and confirmed by thermodynamic predictions. Surface preparation, via grinding with P1200 grit paper, of the AM 316LSS, rather than the use of the native AM surface, disrupts the solidification substructure at the surface.<sup>[20,21]</sup> This substructure has been related to phase transformation suppression in other AM systems.<sup>[20]</sup> Hence, the BCC-Fe layer has formed on the interface with both 316LSS parts in the present example, while in earlier work using the native surface, this was not the case.<sup>[14]</sup> While small, the presence of this BCC-Fe structure at the joint interfaces may impact on the joint performance, either through directly changing the joint mechanics or due to phase changes that could occur with temperature. Such a BCC-Fe layer has been found in multiple brazing systems applied to austenitic stainless steels, and it is therefore critical to understand how it influences the joint strength and failure mechanism.

### 3.2. Joint Strength and Fractography

The design of the test specimen with two similar joints means that, upon sample failure defined as separation of one of the joints, the other joint is still intact. If joint strength is reproducible, the still intact joint was then in the near-failure condition at the point where the test stopped. It can thus be examined for the

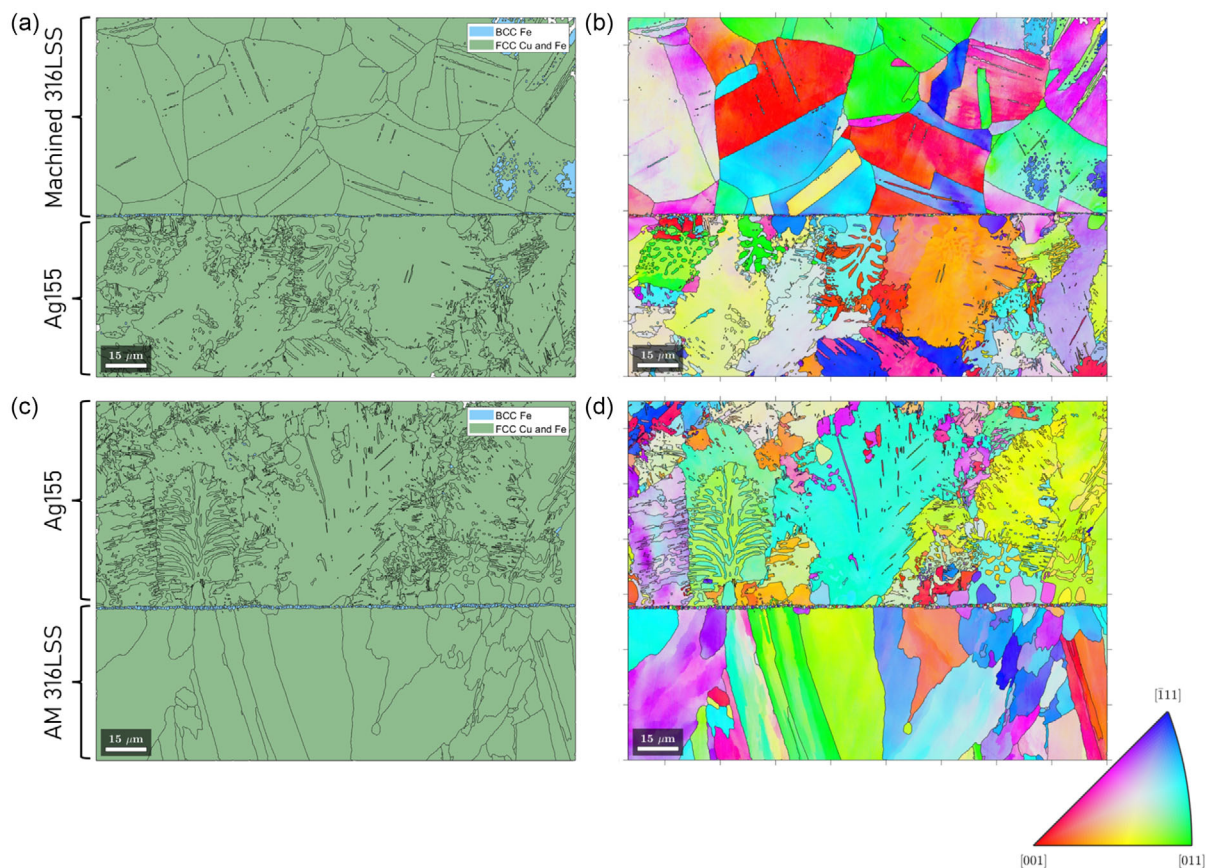


**Figure 3.** EBSD a,c) phase and b,d) inverse pole figure (IPF) maps for the interface region between (a,b) Ag155 and machined 316LSS and (c,d) Ag155 and AM 316LSS.

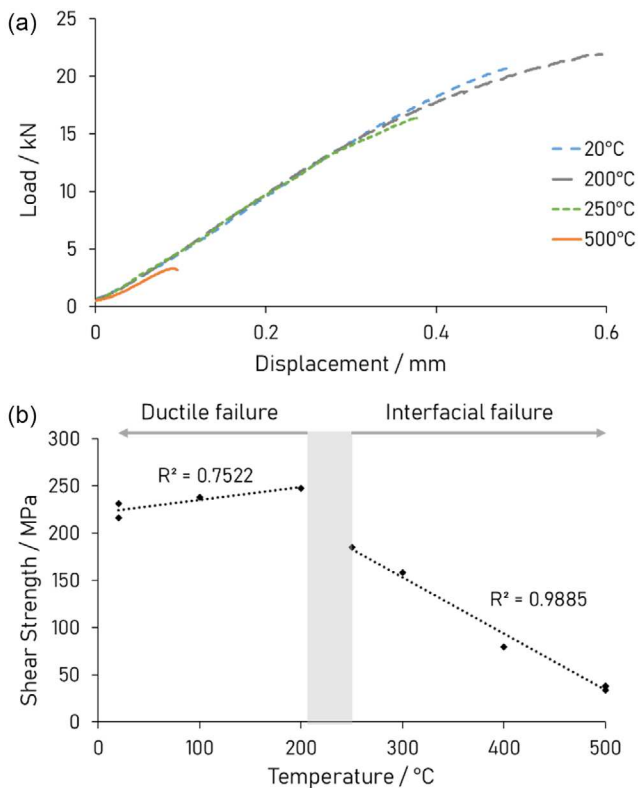


**Figure 4.** a) Force applied versus displacement for various temperatures tested and b) individual data points for shear strength at failure versus temperature for all samples tested.

presence of any build-up of internal damage prior to separation; such intact joints are used later in this work to produce images in Figure 7a,c. To resolve the shear strength from the measured failure load, a value for the joint area is needed. In this work, samples were verified after manufacture to ensure that filler metal was visible along the complete circumference of each joint, signaling that the braze has flowed through the entire joint gap. Note that this does not imply that the joint is entirely filled: Some joint porosity is common in brazing and was observed here (as shown on the fracture surfaces in Figure 5, discussed later). To compute the apparent shear strength of the braze, the maximum total force applied was divided by the total area of both joints. This gives the average shear stress that was applied on either of the two joints at the moment the weaker joint failed. Doing so neglects the influence of edge effects and that of any large-scale pores within the braze (which reduce the effective braze surface area). Braze failure shear stress values reported here are, thus, lower-bound estimates of the local strength of a fully brazed joint and will tend to be lower than the average that might be assessed by other means using a smaller joint area. It is also noted that during testing, joint failure did not consistently occur on the same side of the specimen, indicating that failure is not related to any misalignment in the testing rig.

**Figure 4** shows the relationship between the force applied and displacement recorded at several temperatures. As seen, the slope of the curves for all the datasets is the same, regardless of temperature, suggesting that there is little plastic deformation

or internal damage in the braze alloy prior to failure, and that the measured displacement is initially dominated by the overall load strain compliance. Up to 200 °C, the shear failure strength remains relatively unchanged, noting that apart from the tests at room and 500 °C, repeat samples were not tested, and while the trends in the results appear relatively clear, it is possible that specific features of the joints made, such as defects, have affected the results. It must also be noted that the failure strength, rather than the yield stress, was used in the analysis as the equipment was not fitted with an extensometer to accurately identify the strain within the braze of each sample. Therefore, the margin of error in the estimation of a yield stress was deemed too large for it to be of use.

Macroscopic images of the fracture surface on the AM side of the joint are shown in **Figure 5** for each test temperature. The fact that the samples failed in shear is likely to have caused mutual rubbing of fracture surfaces and obscured features of the fracture surface, such as signs showing the crack path or initiation site; however, these fractographs provide evidence of a change in mechanism with elevated temperature. At temperatures up to 200 °C, there is some filler material present at the surface (i.e., the failure has not happened along the interface between filler and AM 316LSS), and evidence of macroscale ductility can be observed in the filler, with directional plastic deformation visible across the surface. At higher temperatures, the failure tends to occur between the filler and one or other of the 316SS sides of the joint, and evidence of brittle fracture is found, where the interface appears featureless (other than the observation of occasional defects, such as millimeter-scale porosity, the presence of which is typical in brazed joints; this arises during processing). SEM images of the ductile region of the filler metal at the fracture surface are shown in **Figure 6a,b**. The ductile behavior of the filler is evidenced in each micrograph by the presence of microvoid coalescence. Up to 200 °C, there is evidence of shear tearing, consistent with increasing ductility with rising temperature. For 20 °C (and also, slightly less visibly, at 200 °C), the separation between dimples observed is consistent with the microstructural features of the braze alloy, where a Cu-rich phase and eutectic regions, both roughly 20 μm wide, are present within an Ag-rich matrix, as shown in Figure 2.

At 250 °C and above, the fractured surface displays macroscopically a more varied failure mode, with a decreasing proportion of ductile failure surface as the test temperature increases, as seen in Figure 5. At 250 °C, failure occurs at the interfaces between the filler metal and the 316LSS surfaces, with the fracture transitioning between the AM 316LSS/Ag155 filler interface on the left and the machined 316LSS/Ag155 filler interface on the right of the image in Figure 5. From 300 °C to 500 °C, Figure 5 shows that the joint fractography has few features beside the pores that formed during the furnace brazing process within the filler metal. The flat surfaces represent brittle interfacial failure, which occurs between the machined (for joints tested at 300 °C and above) 316LSS and the Ag155 filler metal. Overall, the fractured surfaces show a clear change in failure mechanism, from ductile up to 200 °C, to a brittle interfacial failure at higher temperatures. This in turn correlates with the distinct drop in strength that is seen past 200 °C in the mechanical testing data (Figure 4b). Data suggest a linear trend, although being based on single samples at each temperature apart from 500 °C, the trend must be



**Figure 5.** Photographs of the fractured surfaces taken of the AM 316LSS side of the joint after failure for all temperatures measured. All images show the full 7.5 mm diameter of the specimen. Black circular regions are pores that formed during the furnace brazing process and are typical for such joints. While such defects are candidates for the sites of crack initiation, due to the way the surfaces move past each other during testing, detailed analysis of the crack path and identification of crack initiation sites is not possible.

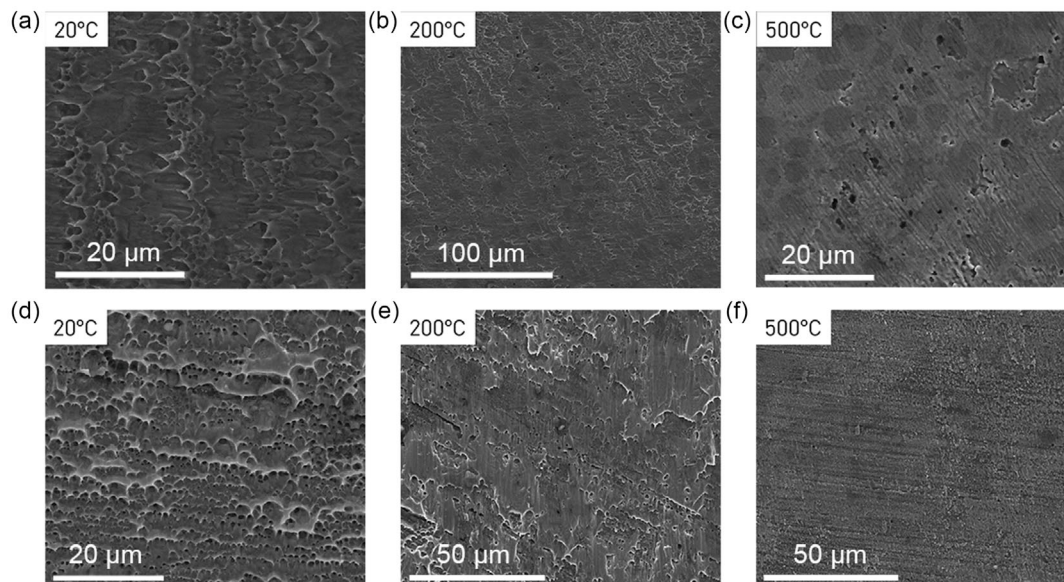


**Figure 6.** SEM images of the post-failure surfaces at various temperatures. Fracture normally occurs close to the interface between the brazing filler metal and one or other of the stainless steel cylinders, and images have been selected to show different sides of these fracture surfaces; the Ag155 side of the fracture surface at a) 20 °C, b) 200 °C, c) 500 °C, and the 316LSS side of a fracture surface (with all examples taken from the machined side of the joint for consistency; this side was the most common, but not exclusive, location for the failure to take place) at d) 20 °C, e) 200 °C, and f) 500 °C.

viewed as tentative. We also note that the three samples at 500 °C show good consistency in the results, given the level of superimposition of data points on the graph. The oxidation visible post-testing in the 300 °C to 500 °C joints (as a discoloration on the fracture surface) is likely a result of the fracture surface being exposed to air post failure at the elevated temperatures and is thus most likely an effect, rather than a cause, of fracture. Supporting evidence for this is that i) this discoloration was

not observed with samples tested at lower temperatures and ii) tests were short and failure was sudden, making it unlikely that crack propagation was driven by a slow chemical crack-tip process such as oxidation.

Variations in the failure mechanism as the temperature increases from 20 to 500 °C are further documented in the SEM micrographs in Figure 6a–f, which focus on the failure surfaces that are seen when fracture occurs at the interface between

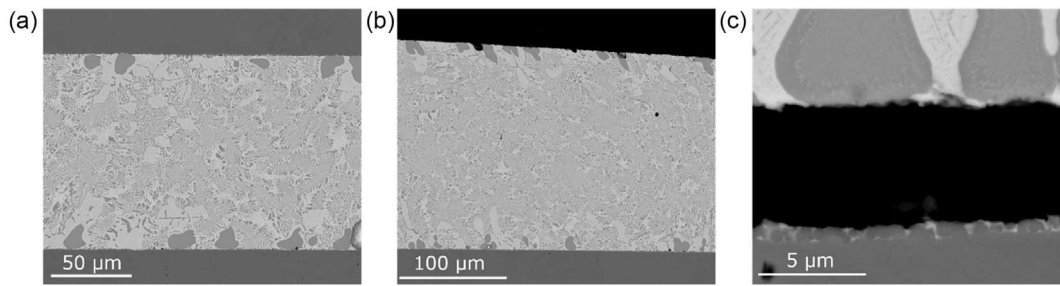


**Figure 7.** SEM images of the post-test Ag155 region on a) 20 °C near-failed joint compared with b) 20 °C failed joint, still attached to the AM 316LSS, and c) 500 °C near-failed joint which was still attached out of plane.

the machined 316LSS and the filler metal. At 20 °C, the fractured surfaces appear ductile on both sides of the joint, with evidence of plastic deformation present along the failure surfaces of both the filler and the 316LSS side of the joint. Some degree of alignment of microvoids parallel to the polished grooves of the base material is found in Figure 6a; likely this is a consequence of the contrast in flow stress between the braze and stainless steel. Localization of ductile deformation at this scale is also induced by the two-phase microstructure of the Ag155 filler, consisting of an Ag-rich phase and a phase containing a larger proportion of Cu,<sup>[1]</sup> with the more highly pure Ag-rich phase likely to be the more ductile.

At 200 °C, the increased ductility, seen in Figure 4a, results in the elongation of the dimples along the shearing direction on the braze side of the fracture surface, Figure 6b. At 500 °C, however, there is no sign of ductility visible along the fracture surface, shown by a featureless surface in Figure 6c. The SEM image in Figure 6c shows that the microstructure of the filler metal, with the darker spots rich in Cu and the lighter matrix rich in Ag, has essentially not been deformed during mechanical testing at 500 °C. On the other side of the fractured joint (Figure 6f), there is no evidence of the presence of the filler metal. This agrees with the macroscopic images in Figure 5, which show brittle interfacial failure above 200 °C. As fracture happens in the same region as the BCC phase occurs, it can be questioned if there is a correspondence between the two, and this can be investigated with examination of the joint cross sections.

As previously mentioned, on the unbroken side, there is also an equivalent joint which has nominally experienced identical loading, but for which unloading has occurred before failure. These joints were also examined in cross section to see what can be learned about the failure processes, with example SEM micrographs shown in Figure 7. Figure 7a,b shows samples tested at 20 °C and compares cross sections through the full joint (showing the filler in the centre, and the 316LSS at the top and bottom) on the side where the joint remained intact in Figure 7a and the side where the joint was fully separated in testing in Figure 7b. The microstructure within the filler does not seem to be affected by the deformation. This suggests that the plastic deformation seen in the 20 °C fracture surface images is confined to the failure region and is not distributed into the depth. It is visible from comparison of Figure 7a,b that at 20 °C, the crack has followed a path situated

at, or near, the interface between the filler and the substrate. The fact that the joint on the side that did not fail at this temperature showed no signs of partial damage suggests that the failure process started at a particular weak flaw on the failed side of that sample.

After testing at higher temperatures, the braze structure remained unchanged and did not show any orientation of the structure, as would be expected to have been produced by extensive plastic flow. Unlike at 20 °C, however, signs of damage in both of the two joints were found. In the samples tested at 500 °C, the nominally intact joint after testing contained a crack that had partially traversed the braze. Figure 7c shows a higher magnification of this crack, including the material on both of its sides, separation of crack sides having not occurred given that the material remained connected out of the imaging plane (the filler is in the top of the image and the 316LSS at the bottom). As seen, the crack path is between the filler metal and what is visible of the fine structured interfacial reaction zone, which was shown to be a transformed, BCC structured, layer. As previously discussed, this transformed layer forms from the 316LSS due to the elemental migration (principally nickel) from the steel to the filler metal. Whether the exact crack path corresponds to the original surface of the 316LSS or to weakness along the interface between the braze alloy and the BCC layer itself cannot be ascertained here; however, the correspondence of the structural change in the material with the brittle failure mode indicates that this change in surface crystalline structure of the 316LSS along the interface with the braze may be undesirable, at least for service under the elevated temperature conditions (300–500 °C) where this behavior was observed.

To close with a few remarks concerning the test procedure adopted here, the present geometry of shear test specimen, shown in Figure 1, was effective for these joints and could be suitable for assessing the properties of other kinds of brazed or soldered joints. As demonstrated, the design is compatible with testing at elevated temperatures and is suitable for use with developmental materials (fillers or substrates) given the small sample sizes involved. Unlike some other existing tests used for these purposes, the design offers the advantages of a symmetrical loading condition and a closer analogue to simple shear at the joint, along with the ability to obtain, from a single sample, both the fracture surfaces and an intact joint at a point just prior to failure, by means of which internal damage processes can be documented.

## 4. Conclusions

In this work, the strength with temperature of a typical brazed joint between AM and machined 316LSS has been examined. Noting that, apart from tests at 20 °C and 500 °C, single samples only are examined at each temperature, the results indicate a significant effect on the joint strength. More specifically, there is a transition in fracture mode and strength past 200 °C. Below 200 °C, the failure strength does not appreciably decline, with shear strength of the braze exceeding 200 MPa. Above 200 °C, the joint strength is found to decrease with increasing temperature, in a generally linear fashion from  $\approx$ 200 to 50 MPa between 200 and 500 °C.

An FCC to BCC transformation of the iron-based material occurs at the interface between the joint and the substrate, similar to what has been documented after brazing austenitic stainless steel using a CuGeNi braze alloy. The formation of this layer can be attributed to the migration of (austenite-stabilizing) nickel from the steel into the copper-based braze during the joining operation. At 500 °C, brittle failure of the brazed joints occurs along the interface between this layer of BCC crystals and the braze alloy. Although there is no direct evidence that this BCC layer is the cause of the failure, its presence might cause the observed transition in fracture mode and braze strength past 200 °C, which should be viewed as a maximum operating temperature for brazes of the type investigated here.

In carrying out the investigation, a new geometry of shear test specimen, giving symmetrical loading, and suitable for relatively small joint sizes, has been shown to be suitable for the testing of brazed joints of the kind examined here, including for elevated temperature testing and allowing the observation of fracture surfaces and an intact joint near to the point of failure.

## Acknowledgements

This work was supported by a UKRI UK-Switzerland collaboration grant, BB/X005046/1. FL would like to acknowledge a studentship provided by the EPSRC through the EPSRC/SFI Centre for Doctoral Training in Advanced Metallic Systems, EP/S022635 AMS3. The authors also wish to acknowledge the Henry Royce Institute for Advanced Materials, funded through EPSRC grants EP/R00661X/1, EP/S019367/1, EP/P02470X/1, and EP/P025285/1, for access to AM equipment at the University of Sheffield.

## Conflict of Interest

The authors declare no conflict of interest.

## Author Contributions

**Frances Livera:** conceptualization (supporting); data curation (lead); formal analysis (lead); investigation (lead); methodology (equal); writing—original draft (lead). **Raphaël Charvet:** investigation (supporting); methodology (equal); writing—review and editing (supporting). **Neil Hind:** investigation (supporting); methodology (equal). **Sophie Barwick:** investigation (supporting). **Dennis Premoli:** investigation (supporting). **Iain Todd:** resources (supporting); supervision (supporting); writing—review and editing (supporting). **Andreas Mortensen:** conceptualization (supporting); methodology (equal); supervision (supporting); writing—review and

editing (supporting). **Russell Goodall:** conceptualization (equal); formal analysis (supporting); funding acquisition (lead); supervision (lead); writing—review and editing (lead).

## Data Availability Statement

The data that support the findings of this study are available from the corresponding author upon reasonable request.

## Keywords

316L stainless steel, additive manufacture, brazing, shear testing

Received: January 31, 2025

Revised: May 2, 2025

Published online:

- [1] M. Way, J. Willingham, R. Goodall, *Int. Mater. Rev.* **2020**, *65*, 257.
- [2] Y. Chen, S. Chen, L. Li, *Mater. Des.* **2010**, *31*, 227.
- [3] Y. Li, X. Zhang, D. Par, S. Jones, B. Chen, *Mater. Charact.* **2019**, *151*, 542.
- [4] Y. Li, D. Parfitt, P. E. J. Flewitt, X. Hou, J. Quinta de Fonseca, B. Chen, *Mater. Sci. Eng. A* **2020**, *796*, 139992.
- [5] S. Zhong, Y. Shi, Y. Li, J. Qin, H. Yu, D. Cui, W. Long, *Nanotechnol. Rev.* **2023**, *12*, 1.
- [6] H. Yu, L. Zhang, F. Cai, S. Zhong, J. Ma, L. Bao, Y. Jiu, B. Hu, S. Wei, W. Long, *Nanotechnol. Rev.* **2020**, *9*, 1034.
- [7] W. Zhu, H. Zhang, C. Guo, Y. Liu, X. Ran, *Vacuum* **2019**, *166*, 97.
- [8] P. Xue, Y. Zou, P. He, Y. Pei, H. Sun, C. Ma, J. Luo, *Metals* **2019**, *9*, 3.
- [9] D. Herzog, V. Seyda, E. Wycisk, C. Emmelmann, *Acta Mater.* **2016**, *117*, 371.
- [10] W. J. Sames, F. A. List, S. Pannala, R. R. Dehoff, S. S. Babu, *Int. Mater. Rev.* **2016**, *61*, 315.
- [11] Y. M. Wang, T. Voisin, J. T. McKeown, J. Ye, N. P. Calta, Z. Li, Z. Zeng, Y. Zhang, W. Chen, T. T. Roehling, R. T. Ott, M. K. Santala, P. J. Depond, M. J. Matthews, A. V. Hamza, T. Zhu, *Nat. Mater.* **2018**, *17*, 63.
- [12] P. Bajaj, A. Hariharan, A. Kini, P. Kurnsteiner, D. Raabe, E. A. Jagle, *Mater. Sci. Eng. A* **2020**, *772*, 1.
- [13] N. Haghdad, M. Laleh, M. Moyle, S. Primig, *J. Mater. Sci.* **2021**, *56*, 64.
- [14] F. S. Livera, *Brazing of Additively Manufactured Metals*, PhD Thesis, Department of Materials Science and Engineering, University of Sheffield **2024**.
- [15] K. Matsu, Y. Miyazawa, Y. Nishi, T. Ariga, *Mater. Trans.* **2007**, *48*, 1055.
- [16] K. Tserpes, A. Barroso-Caro, P. A. Carraro, V. C. Beber, I. Floros, W. Gamon, M. Kozłowski, F. Santandrea, M. Shahverdi, D. Skejić, C. Bedon, V. Rajčić, *J. Adhes.* **2022**, *98*, 1855.
- [17] O. Kozlova, R. Voytovych, M. F. Devismes, N. Eustathopoulos, *Mat. Sci. Eng. A* **2008**, *495*, 96.
- [18] E. M. F. de Souza Silva, G. S. da Fonseca, E. A. Ferreira, *J. Mater. Res. Technol.* **2021**, *15*, 4317.
- [19] D. Sage, C. Fink, *Materialia* **2022**, *24*, 8.
- [20] F. S. H. B. Freeman, J. Sharp, J. Xi, I. Todd, *Addit. Manuf.* **2019**, *30*, 100917.
- [21] Y. Kaynak, O. Kitay, *J. Manuf. Mater. Process.* **2018**, *2*, 36.